 CMES, vol.32, no.1, pp.17-33, 2008

A Numerical Solution of 2D Buckley-Leverett Equation via Gradient Reproducing Kernel Particle Method

Hossein M. Shodja[1,2,3] **and Alireza Hashemian**[1,4]

Abstract: Gradient reproducing kernel particle method (GRKPM) is a meshless technique which incorporates the first gradients of the function into the reproducing equation of RKPM. Therefore, in two-dimensional space GRKPM introduces three types of shape functions rather than one. The robustness of GRKPM's shape functions is established by reconstruction of a third-order polynomial. To enforce the essential boundary conditions (EBCs), GRKPM's shape functions are modified by transformation technique. By utilizing the modified shape functions, the weak form of the nonlinear evolutionary Buckley-Leverett (BL) equation is discretized in space, rendering a system of nonlinear ordinary differential equations (ODEs). Subsequently, Gear's method is applied for temporal discretization of the ODEs. Through numerical experiments, employment of a moderate viscosity seeks the efficacy of the solution when the diffusion term is important; moreover, application of a small viscosity confirms the potential of the approach for treatment of the problems involving steep gradient regions. The outcomes are verified by performing convergence tests using uniformly spaced particles. Consideration of non-uniform distribution of particles further demonstrates the virtue of the presented methodology in producing smooth profiles in the critical regions near the fronts.

[1] Center of Excellence in Structures and Earthquake Engineering, Department of Civil Engineering, Sharif University of Technology, P.O. Box 11155-9313, Tehran, Iran

[2] Institute for Nanoscience and Nanotechnology, Sharif University of Technology, P.O. Box 11155-9161, Tehran, Iran

[3] Corresponding author. Tel: (+98-21) 6616-4209; Fax: (+98-21) 6601-4828. E-mail: shodja@sharif.edu (H. M. Shodja)

[4] Email: al.hash@gmail.com (A. Hashemian).

Keyword: Buckley-Leverett equation; Gradient reproducing kernel particle method; Steep gradient; Two-phase flow; Meshless; Nonlinear evolutionary partial differential equation

1 Introduction

Multiphase flow through porous media is a class of nonlinear hydrodynamical systems which has become an important topic in various areas of science and engineering in recent years. Examples include the exploitation of natural resources, and a remedy to the environmental problem of contaminated sites, [Parker (1989)]. Multiphase flow occurs when the fluids are immiscible and are separated by a sharp interface on the pore scale. For example, the immiscible displacement of oil (non-wetting fluid) from a porous medium by water (wetting fluid) is extensively used in the petroleum industry. This is done by frequent injection of water into the reservoir to displace the oil [Aziz and Settari (1979)]. Polymer flooding is an alternative to water flooding for enhanced oil recovery.

The saturation of a two-phase flow in a porous medium when neglecting the gravitational and capillary forces is modeled by the classical Buckley-Leverett (BL) equation, [Buckley and Leverett (1942)],

$$\dot{u} + \nabla.[f(u)] = 0, \tag{1}$$

where $u = u(\mathbf{x},t)$, $\mathbf{x} \in \Omega$, $t > 0$, $\dot{u} = \frac{\partial u}{\partial t}$, and

$$f(u) = \frac{u^2}{u^2 + \alpha(1-u)^2}, \tag{2}$$

in which α is an specified parameter expressing the ratio of the fluids' viscosities. In the case of oil and water flowing through sand, the dependent variable u describes the water saturation of

the sand, and f is a flux function of the flowing stream. The high nonlinearity of f is characterized by formation of a front which becomes steeper as it advances in the domain with the evolution of u, and eventually becomes a shock.

Many systems in fluid dynamics, meteorology, astrophysics, petroleum reservoir simulation, etc., are viscous and modeled by

$$\dot{u} + \nabla.[f(u)] = \nu \nabla^2 u, \tag{3}$$

where $\nu > 0$ represents the viscosity of the system. Moreover, the true solutions of the inviscid hyperbolic Eq. (1) develop truly infinite gradients in u and thereafter continue to exist only as weak (non-classical) solutions which are the limits of the viscous solutions, as the viscous term tends to zero, [Gelinas, Doss, and Miller (1981)].

Numerical analysis of the viscous systems are difficult because of the high gradients, albeit finite, in the solution of u. It is not our purpose to exhaust all the numerical schemes. Nevertheless, the existing numerical methods commonly used in industry are finite difference (FD), finite volume (FV), and finite element (FE) methods. FD technique is efficient on regular structured grids, but loses its stability on unstructured meshes. FV method is of low order. The classical FE method is also inadequate to model sharp fronts and results in overshooting and undershooting, particularly in the vicinity of the fronts. Among the numerical remedies, adaptive mesh refinement in FD; for example [Berger and Oliger (1984)], or moving FE; for example [Gelinas, Doss, and Miller (1981)] and [Johnson, Wathen, and Baines (1988)] had been designed to capture such fronts. Discontinuous Galerkin method which supports local approximations of high gradients is another methodology for porous medium flow calculations, see [Rivière and Bastian (2004)].

Meshless technique is a modern approach which has proved useful for handling problems exhibiting discontinuities, high gradients, severe deformations, or moving boundaries. Since there is no explicit mesh, time and error involved in meshing procedures are eliminated. Moreover, there is no concern about formation of awkward elements. In the literature, several meshless methods have been proposed; for example, smooth particle hydrodynamics (SPH) by Lucy (1977), diffuse element method by Nayroles, Touzot, and Villon (1992), element free Galerkin method (EFGM) by Belytschko, Lu, and Gu (1994a), reproducing kernel particle method (RKPM) by Liu, Jun, and Zhang (1995), hp-clouds method by Durate and Oden (1996), partition of unity method by Babuška and Melenk (1997), local boundary integral equation method by Zhu, Zhang, and Atluri (1998a, b), meshless local Petrov-Galerkin method (MLPG) by Atluri and Zhu (1998). Various MLPG methods are discussed comprehensively by Atluri and Shen (2002a, b). A review of meshless techniques and their applications may be found in Li and Liu (2002).

Some authors took advantage of the Hermite interpolation and incorporated the derivative(s) of the function in their approximations. Among the contributions which follow this school of thought, the work of Liu, Chen, Uras, and Chang (1996) in Hermite reproducing kernel method; Atluri, Cho, and Kim (1999) in generalized moving least square (GMLS); Li, NG, Cheng, and Lam (2003) in Hermite-cloud method should be mentioned. Atluri, Cho, and Kim (1999) employed GMLS approximation to analyze the bending problem of thin beams. Later, Cho and Atluri (2001) extended the work of Atluri, Cho, and Kim (1999) to the shear flexible beams based on a locking-free formulation. Raju and Phillips (2003) applied the GMLS approximation to a continuous beam problem and gave a complete discussion on the effects of various parameters on the numerical results. It should be noted that 4th order problems can be treated without incorporating the derivative(s) of the function in the interpolation; for example, the bending problem of a thin plate [Long and Atluri (2002)] and a 4th order ODE [Atluri and Shen (2005)] were solved by moving least square (MLS) approximation.

For the conventional symmetric weak forms of a 4th order differential equation, the trial function should have C^1 continuity in the domain of integration; see [Long and Atluri (2002)]. However, by employing mixed MLPG approach only C^0 continuity is sufficient; see [Atluri and Shen

(2005)]. In the mixed approach, displacements as well as displacement gradients are interpolated independently using identical MLS shape functions. Subsequently, the weak form contains only the displacements instead of explicit involvement of the displacement gradients. Three mixed MLPG methods have been developed: i) MLPG mixed finite volume by Atluri, Han, and Rajendran (2004); ii) MLPG mixed collocation by Atluri, Liu, and Han (2006a); and iii) MLPG mixed finite difference by Atluri, Liu, and Han (2006b). The differences between these schemes include defining local sub-domains, employing local weak forms, choosing trial and test functions, and utilizing differential operators.

It is well-known that enforcement of essential boundary conditions (EBCs) by the conventional meshless methods such as RKPM is problematic. This dilemma has been the subject of several contributions. The corrected collocation method (CCM) proposed by Wagner and Liu (2000), however efficient, is not applicable to the derivative type of EBCs. For this reason, Hashemian (2000) generalized the CCM to enforce not only the function but also the derivative type of EBCs. To this end, the gradient term was introduced into the reproducing equation, which entailed a new formulation of RKPM and the CCM. This new approach, because of the added gradient term in the reproducing equation is called the gradient RKPM (GRKPM), [Shodja and Hashemian (2007a); Hashemian and Shodja (2008a)]. The advantage of GRKPM over the conventional RKPM is that, in addition to the exact enforcement of the EBCs, without resorting to such techniques as Lagrange multipliers [Belytschko, Lu, and Gu (1994a)] or penalty [Belytschko, Lu, and Gu (1994b); Zhu and Atluri (1998)], it leads to much more accurate results and higher convergence rates [Shodja and Hashemian (2007a); Hashemian and Shodja (2008a)]. The efficacy of GRKPM in handling problems involving the second derivatives of the unknown functions in their weak formulations is investigated by employing it to thin beam-columns and plates [Shodja and Hashemian (2007a, b); Hashemian and Shodja (2008a)]. The high performance and accurate resolution of GRKPM when dealing with the Burgers' equation exhibiting evolutionary high gradients and shocks suggest that it has the potential to be employed to other areas of computational physics where the numerical solution of nonlinear evolutionary partial differential equations is desired, [Hashemian and Shodja (2008b)].

In the present work, we consider the viscous BL equation, Eq (3), in two-dimensional Euclidian space with $\alpha = \frac{3}{4}$; see Eq. (2). The associated initial and boundary conditions, which were previously utilized by Johnson, Wathen, and Baines (1988), are assumed

$$u(\mathbf{x},0) = \frac{0.1}{0.1 + \frac{1}{4}\sqrt{x_1^2 + x_2^2}}, \quad \mathbf{x} \in \Omega \cup \Gamma, \tag{4}$$

$$u(\mathbf{0},t) = 1, \tag{5a}$$

$$\frac{\partial u}{\partial n} = 0 \quad \text{on } \Gamma - \{0\}, \tag{5b}$$

in which $t > 0$, $\Omega = (0,4)^2$, Γ is the boundary of Ω, and $\mathbf{n}$ is the unit outward normal to Γ. Note that Eq. (5a) is the EBC and Eq. (5b) represents the natural boundary condition.

The outline of this paper is as follows. In section 2, two dimensional formulation of GRKPM is elucidated in details and the reconstruction property of GRKPM is well illustrated. Section 3 is devoted to discretization. Numerical experiments are provided in section 4 where two very different values of viscosity are investigated. Employment of a moderate viscosity seeks the efficacy of the solution when the diffusion term is important, whereas application of a small viscosity confirms the potential of the approach for the treatment of the problems involving steep gradient regions. Moreover, non-uniform distribution of particles is considered for exploring the performance of the proposed method. Finally, conclusions are remarked in section 5.

2 2D GRKPM

2.1 The reproducing equation

The reproducing equation in terms of the function and its first gradients is defined as

$$u^R(\mathbf{x},t)=\sum_{k=0}^{2}\int_\Omega \overline{\phi}_a^{[k]}(\mathbf{x};\mathbf{x}-\mathbf{y})u_{,k}(\mathbf{y},t)d\mathbf{y}, \tag{6}$$

in which Ω is the 2-D space, t is time, $u^R(\mathbf{x},t)$ is the reproduced function, $u_{,0}=u$, $u_{,k}(\mathbf{y},t)=\frac{\partial u(\mathbf{y},t)}{\partial y_k}, k=1,2$, and $\overline{\phi}_a^{[k]}(\mathbf{x};\mathbf{x}-\mathbf{y})$ is the modified kernel function associated with $u_{,k}$. As mentioned earlier, the conventional RKPM is based on the reproducing equation in the absence of the gradient terms. The inclusion of the gradient terms requires a complete reformulation and circumvention of some new obstacles which are discussed in the following.

The modified kernel functions are defined as

$$\overline{\phi}_a^{[0]}(\mathbf{x};\mathbf{x}-\mathbf{y})=\left[b_0(\mathbf{x})+\sum_{i=1}^{2}b_i(\mathbf{x})(x_i-y_i)\right]\phi_a(\mathbf{x}-\mathbf{y}), \tag{7a}$$

$$\overline{\phi}_a^{[k]}(\mathbf{x};\mathbf{x}-\mathbf{y})=\left[b_k(\mathbf{x})+\sum_{i=1}^{2}b_{ki}(\mathbf{x})(x_i-y_i)\right]\phi_a(\mathbf{x}-\mathbf{y}),\quad k=1,2. \tag{7b}$$

The unknown coefficients $b_0(\mathbf{x})$, $b_k(\mathbf{x})$ and $b_{ki}(\mathbf{x})$, $k,i=1,2$ with $b_{12}=b_{21}$ are obtained through completeness requirements. The kernel function $\phi_a(\mathbf{x}-\mathbf{y})$ is given by

$$\phi_a(\mathbf{x}-\mathbf{y})=\prod_{i=1}^{2}\frac{\phi(z_i)}{a_i}, z_i=\frac{x_i-y_i}{a_i}, \tag{8}$$

where $\phi(z)$ is the so-called window function. In this paper $\phi(z)$ is taken to be a cubic spline defined as

$$\phi(z)=\begin{cases}\frac{2}{3}-4z^2+4z^3 & 0\le|z|\le\frac{1}{2}\\ \frac{4}{3}-4z+4z^2-\frac{4}{3}z^3 & \frac{1}{2}<|z|\le 1\\ 0 & \text{otherwise}\end{cases}. \tag{9}$$

Substitution of (7) in (6) gives,

$$u^R(\mathbf{x},t)=\int_\Omega[b_0(\mathbf{x})+\sum_{i=1}^{2}b_i(\mathbf{x})(x_i-y_i)]\phi_a(\mathbf{x}-\mathbf{y})u(\mathbf{y},t)d\mathbf{y}+\sum_{k=1}^{2}\int_\Omega[b_k(\mathbf{x})+\sum_{i=1}^{2}b_{ki}(\mathbf{x})(x_i-y_i)]\phi_a(\mathbf{x}-\mathbf{y})u_{,k}(\mathbf{y},t)d\mathbf{y}. \tag{10}$$

2.2 Determination of the unknown coefficients

Consider the Taylor series of u around an arbitrary point $\mathbf{x}$ up to the second derivatives

$$u(\mathbf{y},t)\cong u(\mathbf{x},t)-\sum_{p=1}^{2}(x_p-y_p)u_{,p}(\mathbf{x},t)+\frac{1}{2}\sum_{p=1}^{2}\sum_{q=1}^{2}(x_p-y_p)(x_q-y_q)u_{,pq}(\mathbf{x},t). \tag{11}$$

Replacement of (11) in the reproducing equation (10), leads to

$$u^R(\mathbf{x},t)=u(\mathbf{x},t)R_0(\mathbf{x})-\sum_{p=1}^{2}u_{,p}(\mathbf{x},t)R_p(\mathbf{x})+\frac{1}{2}\sum_{p=1}^{2}\sum_{q=1}^{2}u_{,pq}(\mathbf{x},t)R_{pq}(\mathbf{x})+Err, \tag{12}$$

where Err denotes the cumulative truncation error, and

$$\mathbf{R}(\mathbf{x})=\mathbf{M}(\mathbf{x})\boldsymbol{\beta}(\mathbf{x}) \tag{13}$$

where

$$\mathbf{R}^T(\mathbf{x})=\begin{bmatrix}R_0 & R_1 & R_2 & R_{11} & R_{12} & R_{22}\end{bmatrix}, \tag{14}$$

$$\mathbf{M}(\mathbf{x}) = \begin{bmatrix} m_{00} & m_{10} & m_{01} \\ m_{10} & m_{20}-m_{00} & m_{11} \\ m_{01} & m_{11} & m_{02}-m_{00} \\ m_{20} & m_{30}-2m_{10} & m_{21} \\ m_{11} & m_{21}-m_{01} & m_{12}-m_{10} \\ m_{02} & m_{12} & m_{03}-2m_{01} \end{bmatrix} \begin{bmatrix} 0 & 0 & 0 \\ -m_{10} & -m_{01} & 0 \\ 0 & -m_{10} & -m_{01} \\ -2m_{20} & -2m_{11} & 0 \\ -m_{11} & -m_{02}-m_{20} & -m_{11} \\ 0 & -2m_{11} & -2m_{02} \end{bmatrix}, \quad (15)$$

$$\boldsymbol{\beta}^{\mathrm{T}}(\mathbf{x}) = \begin{bmatrix} b_0(\mathbf{x}) & b_1(\mathbf{x}) & b_2(\mathbf{x}) & b_{11}(\mathbf{x}) & b_{12}(\mathbf{x}) & b_{22}(\mathbf{x}) \end{bmatrix}. \quad (16)$$

In (15), $m_{ij}(\mathbf{x})$ is defined as the ijth moment of the kernel function at the point $\mathbf{x}$,

$$m_{ij}(\mathbf{x}) = \int_{\Omega} (x_1-y_1)^i (x_2-y_2)^j \phi_a(\mathbf{x}-\mathbf{y}) d\mathbf{y}. \quad (17)$$

In order to satisfy the completeness requirements pertinent to $u^R(\mathbf{x},t)$, the condition

$$\mathbf{R}^{\mathrm{T}}(\mathbf{x}) = \begin{bmatrix} 1 & 0 & 0 & 0 & 0 & 0 \end{bmatrix}, \quad (18)$$

must be satisfied. In view of Eqs. (13) and (18), the unknown coefficients $b_k(\mathbf{x})$ and $b_{ki}(\mathbf{x})$ are obtained.

The first derivatives of the unknown coefficients, are given by

$$\mathbf{M}(\mathbf{x})\boldsymbol{\beta}_{,r}(\mathbf{x}) = -\mathbf{M}_{,r}(\mathbf{x})\boldsymbol{\beta}(\mathbf{x}), \quad r = 1,2. \quad (19)$$

2.3 The shape functions

Numerical computations of the unknown coefficients $\boldsymbol{\beta}(\mathbf{x})$ and its derivatives require numerical computations of the moments and subsequently discretization of the integral in Eq. (17). To satisfy the consistency conditions the same rule should be used for numerical integration in Eqs. (10) and (17), [Chen, Pan, Wu, and Liu (1996)]. To this end, the trapezoidal rule is employed. Thus Eq. (10) is discretized in the following manner

$$u^R(\mathbf{x},t) = \sum_{J=1}^{NP} \sum_{k=0}^{2} \psi_J^{[k]}(\mathbf{x}) u_{J,k}(t), \quad (20)$$

where NP is the number of particles,

$$u_{J,0}(t) = u(\mathbf{y},t)|_{\mathbf{y}=\mathbf{y}_J}, \quad (21a)$$

$$u_{J,k}(t) = \frac{\partial u(\mathbf{y},t)}{\partial y_k}|_{\mathbf{y}=\mathbf{y}_J}, \quad k = 1,2, \quad (21b)$$

$\psi_J^{[k]}(\mathbf{x})$ is the value of the kth shape function associated with the Jth particle measured at the point $\mathbf{x}$

$$\psi_J^{[0]}(\mathbf{x}) = [b_0(\mathbf{x}) + \sum_{i=1}^{2} b_i(\mathbf{x})(x_i - y_{Ji})]\phi_a(\mathbf{x}-\mathbf{y}_J)\Delta\mathbf{y}_J, \quad (22a)$$

$$\psi_J^{[k]}(\mathbf{x}) = [b_k(\mathbf{x}) + \sum_{i=1}^{2} b_{ki}(\mathbf{x})(x_i - y_{Ji})]\phi_a(\mathbf{x}-\mathbf{y}_J)\Delta\mathbf{y}_J, \quad k = 1,2, \quad (22b)$$

in which $\Delta\mathbf{y}_J$ is the area belonging to the Jth particle. From Eq. (22) it is observed that there are 3 types of shape function $\psi_J^{[k]}(\mathbf{x}), k = 0,1,2$ in 2D GRKPM, Figs. 1–3. Whereas, in RKPM only one type of shape function $\psi_J(\mathbf{x})$ is encountered, Fig. 4. In these figures, 11×11 particles are distributed uniformly in the region $[0,10]^2$. The dilation parameter is $a = 2$. In each figure the shape functions associated with the corner particle $(0,0)$, the edge particles $(5,0)$, $(0,5)$ and the middle particle $(5,5)$ are plotted. It is interesting to note that, the type 1 shape functions in GRKPM are the same as the shape functions in RKPM and differ only in amplitudes for the boundary particles which are affected by the correction functions. Moreover, the type 3 shape functions corresponding to the points $(5,5)$ and $(5,0)$, respectively, can be obtained by 90° counter-clockwise rotation of the type 2 shape functions associated with the particles $(5,5)$ and $(0,5)$ about the line

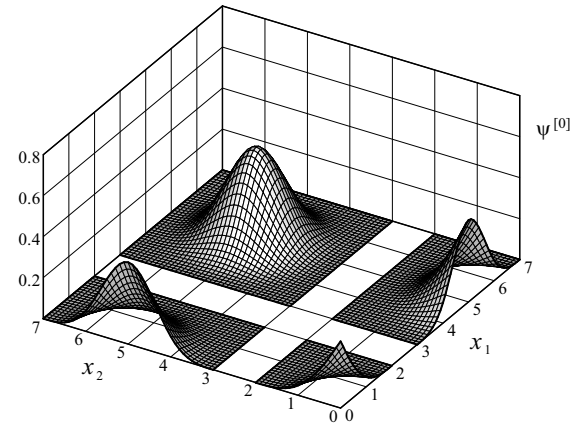

Figure 1: GRKPM shape functions; type 1

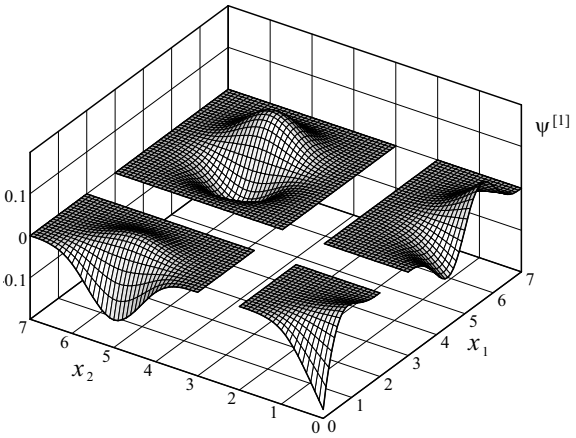

Figure 2: GRKPM shape functions; type 2

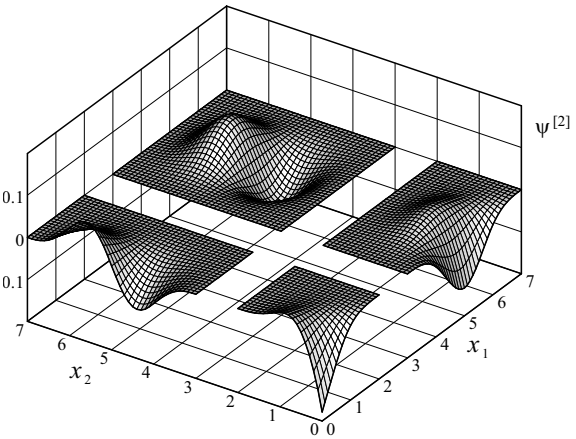

Figure 3: GRKPM shape functions; type 3

perpendicular to the x_1x_2-plane at the point $(5,5)$.

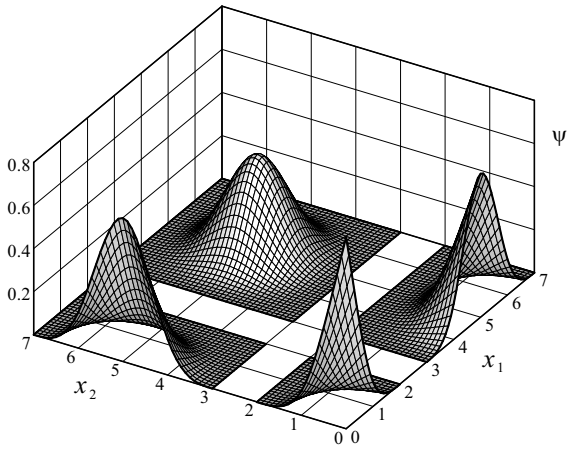

Figure 4: RKPM shape functions

It is also desirable to calculate the first derivatives of the shape functions

$$\left[\psi_J^{[k]}(\mathbf{x})\right]_{,m} = \left\{[b_0(\mathbf{x})]_{,m} + \sum_{i=1}^{2}[b_i(\mathbf{x})]_{,m}(x_i - y_{Ji}) + b_m(\mathbf{x})\right\} \phi_a(\mathbf{x}-\mathbf{y}_J)\Delta\mathbf{y}_J + [b_0(\mathbf{x}) + \sum_{i=1}^{2} b_i(\mathbf{x})(x_i - y_{Ji})][\phi_a(\mathbf{x}-\mathbf{y}_J)]_{,m}\Delta\mathbf{y}_J, \tag{23a}$$

$$\left[\psi_J^{[k]}(\mathbf{x})\right]_{,m} = \left\{[b_k(\mathbf{x})]_{,m} + \sum_{i=1}^{2}[b_{ki}(\mathbf{x})]_{,m}(x_i - y_{Ji}) + b_{km}(\mathbf{x})\right\} \phi_a(\mathbf{x}-\mathbf{y}_J)\Delta\mathbf{y}_J + [b_k(\mathbf{x}) + \sum_{i=1}^{2} b_{ki}(\mathbf{x})(x_i - y_{Ji})][\phi_a(\mathbf{x}-\mathbf{y}_J)]_{,m}\Delta\mathbf{y}_J, \quad k = 1,2, \tag{23b}$$

where $J = 1,2,...,NP$ and $m = 1,2$.

2.4 Function Reconstruction

An immediate implication of Eq. (20) lies in its ability to approximate a function whose values at some given points are known. For demonstration, consider the following polynomial

$$u(\mathbf{x}) = x_1^3 + x_1^2x_2 + x_1x_2^2 + x_2^3, \quad \mathbf{x} \in [0,1]^2. \tag{24}$$

The function $u(\mathbf{x})$ is reproduced by employing different arrays of uniformly distributed particles ranging from 4×4 to 166×166. Hence, the number of particles varies from 16 to 27556. Let Δx be the distance between two adjacent particles in each direction. The dilation parameter is assumed to be $\tilde{a}\Delta x$. By selecting $\tilde{a}$= 1.6, 1.8, and 2.0, the influence of the dilation parameter on convergence behavior is investigated. The accuracy of the results is verified by computing the L_2 norm of the error as

$$\left\|u^R-u\right\|=\sqrt{\int_0^1\int_0^1[u^R(\mathbf{x})-u(\mathbf{x})]^2dx_1dx_2}. \tag{25}$$

The variation of the error with the number of degrees of freedom (DOF) has been computed for both RKPM and GRKPM and is demonstrated in Fig. 5. It is observed that both RKPM and GRKPM display convergence behavior. However, for all the displayed cases the convergence rate for GRKPM is double as compared with the RKPM results. Moreover, the error associated with 768 DOF (256 particles) in GRKPM is even less than the error pertinent to 27556 DOF (27556 particles) in RKPM. It is evident that for both RKPM and GRKPM $\tilde{a}$=2.0 leads to a more accurate result than $\tilde{a}$=1.8 and 1.6. Meanwhile, $\tilde{a}$=1.8 works better than $\tilde{a}$=1.6. It is interesting to note that the convergence rate is almost independent of $\tilde{a}$ for both methods.

Fig. 6 compares the CPU time due to RKPM and GRKPM. It is noted that for the same number of DOF, GRKPM is slightly more time consuming than RKPM. It is noteworthy to mention that the CPU time expended for 27556 DOF (27556 particles) in RKPM is nearly 30 times the CPU time associated with 1587 DOF (529 particles) in GRKPM. Moreover, the results shown in Fig. 5 reveal that the error pertinent to 27556 DOF in the conventional RKPM is about 6 times the error corresponding to 1587 DOF in GRKPM. This verifies the goodness of GRKPM's shape functions and establishes the efficacy of GRKPM in function reconstruction.

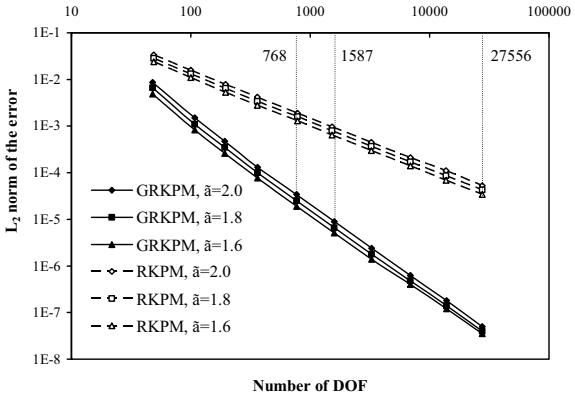

Figure 5: L_2 norm of the error associated with the reproducing of the third order polynomial, Eq. (24)

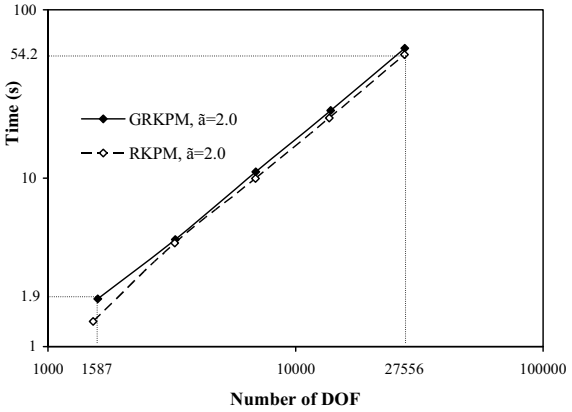

Figure 6: CPU time associated with the reproducing of the third order polynomial, Eq. (24)

2.5 Imposition of the EBC

In the conventional meshless techniques such as those build upon moving least square or reproducing kernel approximation, imposition of EBCs is not as straightforward as in FE-based methods. Because the shape functions of these classes of meshless methods do not have the delta Kronecker property, the prescribed value associated with an EBC is not equal to the value of the pertinent DOF, but rather a linear combination of values corresponding to the DOF of the neighboring particles. To overcome this critical issue, various attempts have been made in the literature. One efficient method to enforce EBCs is the transformation technique which was first proposed by

Chen, Pan, Wu, and Liu (1996) and reiterated by many authors. In the present work, the transformation concept is employed to modify GRKPM's shape functions so that they can have the delta-Kronecker property for the boundary particle and subsequently the EBC, Eq. (5a), can be enforced as conveniently as in FE-based methods. To this end, the discretized equation (20) is rewritten as

$$u(\mathbf{x},t) = \psi_1^{[0]}(\mathbf{x})d_1^{[0]}(t) + \sum_{k=1}^{2} \psi_1^{[k]}(\mathbf{x})d_1^{[k]}(t) + \sum_{J=2}^{NP}\sum_{k=0}^{2} \psi_J^{[k]}(\mathbf{x})d_J^{[k]}(t). \quad (26)$$

Writing Eq. (26) for the boundary point, $\mathbf{x} = \mathbf{0}$, and using Eq. (5a) give

$$d_1^{[0]}(t) = \frac{1}{\psi_1^{[0]}(\mathbf{0})} - \sum_{k=1}^{2} \frac{\psi_1^{[k]}(\mathbf{0})}{\psi_1^{[0]}(\mathbf{0})} d_1^{[k]}(t) - \sum_{J=2}^{NP}\sum_{k=0}^{2} \frac{\psi_J^{[k]}(\mathbf{0})}{\psi_1^{[0]}(\mathbf{0})} d_J^{[k]}(t). \quad (27)$$

Substitution of this result into Eq. (26) yields

$$u(\mathbf{x},t) = \overline{\psi}_1^{[0]}(\mathbf{x}) + \sum_{k=1}^{2} \overline{\psi}_1^{[k]}(\mathbf{x})d_1^{[k]}(t) + \sum_{J=2}^{NP}\sum_{k=0}^{2} \overline{\psi}_J^{[k]}(\mathbf{x})d_J^{[k]}(t), \quad (28)$$

where $\overline{\psi}_J^{[k]}(\mathbf{x})$ is the modified shape function pertinent to $\psi_J^{[k]}(\mathbf{x})$

$$\overline{\psi}_1^{[0]}(\mathbf{x}) = \frac{\psi_1^{[0]}(\mathbf{x})}{\psi_1^{[0]}(\mathbf{0})} \quad , \quad (29a)$$

$$\overline{\psi}_1^{[k]}(\mathbf{x}) = \psi_1^{[k]}(\mathbf{x}) - \frac{\psi_1^{[k]}(\mathbf{0})}{\psi_1^{[0]}(\mathbf{0})}\psi_1^{[0]}(\mathbf{x}), \quad k = 1,2, \quad (29b)$$

$$\overline{\psi}_J^{[k]}(\mathbf{x}) = \psi_J^{[k]}(\mathbf{x}) - \frac{\psi_J^{[k]}(\mathbf{0})}{\psi_1^{[0]}(\mathbf{0})}\psi_1^{[0]}(\mathbf{x}), \quad J = 2,3,\ldots,NP, \quad k = 0,1,2. \quad (29c)$$

Application of these modified shape functions ensures the exact enforcement of the EBC in a straight forward manner.

As discussed in the previous section, the shape function $\psi_J^{[k]}(\mathbf{x})$ is compact supported. From Eqs. (29a–c), it can be inferred that the modified shape function, $\overline{\psi}_J^{[k]}(\mathbf{x})$, is also compact supported. Moreover, the domains on which $\psi_J^{[k]}(\mathbf{x})$ and $\overline{\psi}_J^{[k]}(\mathbf{x})$ exert their influences are the same.

3 Discretization of the problem

The necessary space and time discretizations are done via GRKPM and backward differentiation formula (BDF) scheme, respectively. The discretization in space is elucidated in section 3.1. Meanwhile, the temporal discretization is given in section 3.2.

3.1 Discretization in space via GRKPM

Eq. (28) can be read as

$$u(\mathbf{x},t) = \overline{\psi}_{\mathrm{b}}(\mathbf{x}) + \overline{\boldsymbol{\psi}}_{\mathrm{nb}}(\mathbf{x})\mathbf{d}_{\mathrm{nb}}(t), \quad (30)$$

in which

$$\overline{\psi}_b(\mathbf{x}) = \overline{\psi}_1^{[0]}(\mathbf{x}), \quad (31a)$$

$$\overline{\boldsymbol{\psi}}_{\mathrm{nb}}(\mathbf{x}) = \left[\overline{\psi}_1^{[1]}(\mathbf{x})\overline{\psi}_1^{[2]}(\mathbf{x}) \quad \overline{\psi}_2^{[0]}(\mathbf{x})\overline{\psi}_2^{[1]}(\mathbf{x})\overline{\psi}_2^{[2]}(\mathbf{x}) \quad \cdots \quad \overline{\psi}_{NP}^{[0]}(\mathbf{x})\overline{\psi}_{NP}^{[1]}(\mathbf{x})\overline{\psi}_{NP}^{[2]}(\mathbf{x})\right], \quad (31b)$$

$$\mathbf{d}_{\mathrm{nb}}(t) = \left[d_1^{[1]}(t)d_1^{[2]}(t) \quad d_2^{[0]}(t)d_2^{[1]}(t)d_2^{[2]}(t) \quad \cdots \quad d_{NP}^{[0]}(t)d_{NP}^{[1]}(t)d_{NP}^{[2]}(t)\right]^{\mathrm{T}}. \quad (31c)$$

Let $w(\mathbf{x},t)$ be a test function satisfying the homogeneous boundary conditions,

$$w(\mathbf{0},t) = 0. \quad (32)$$

Multiplying the residual associated with the Eq. (3) by w and integrating over the domain, $\Omega = (0,4)^2$, give

$$\int_\Omega w(\dot{u} + f_{,1} + f_{,2} - \nu\nabla^2 u)d\Omega = 0. \quad (33)$$

Integrating by parts, and using (32) along with the natural boundary condition, Eq. (5b), yield

$$\int_\Omega w(\dot{u}+f'u_{,1}+f'u_{,2})d\Omega + \nu\int_\Omega (w_{,1}u_{,1}+w_{,2}u_{,2})d\Omega = 0, \quad (34)$$

where $f' = f'(u) = \frac{df}{du}$. Upon discretization of $w(\mathbf{x},t)$ in the manner utilized in arriving at the discretized expression (30) for $u(\mathbf{x},t)$

$$w(\mathbf{x},t) = \overline{\boldsymbol{\psi}}_{\rm nb}(\mathbf{x})\mathbf{c}_{\rm nb}(t). \quad (35)$$

Since w has arbitrary values at $[0,4]^2-\{\mathbf{0}\}$, $\mathbf{c}_{\rm nb}(t)$ is also arbitrary. Therefore, substitution of Eqs. (35) and (30) into (34) yields

$$\mathbf{E}\dot{\mathbf{d}}_{\rm nb} = \mathbf{g}, \quad (36)$$

where

$$\mathbf{E} = \int_\Omega \overline{\boldsymbol{\psi}}_{\rm nb}^{\rm T}\overline{\boldsymbol{\psi}}_{\rm nb}d\Omega, \quad (37a)$$

$$\mathbf{g} = -\int_\Omega \overline{\boldsymbol{\psi}}_{\rm nb}^{\rm T}(u_{,1}+u_{,2})f'd\Omega - \nu\int_\Omega (\overline{\boldsymbol{\psi}}_{\rm nb,1}^{\rm T}u_{,1}+\overline{\boldsymbol{\psi}}_{\rm nb,2}^{\rm T}u_{,2})d\Omega. \quad (37b)$$

The integrations in Eqs. (37a) and (37b) is calculated numerically by employing the standard Gaussian quadrature scheme. To this end, a background mesh is constructed by drawing imaginary grid lines through the particles pertinent to GRKPM. In this manner the domain is hypothetically subdivided into a number of cells. Subsequently, for the integration purposes a 4×4 quadrature is considered for each cell.

Solution of Eq. (36) which consists of $NP-1$ nonlinear ODEs requires the availability of $NP-1$ initial conditions (ICs). In view of Eqs. (30) and (4)

$$\overline{\psi}_b(\mathbf{x}) + \overline{\boldsymbol{\psi}}_{\rm nb}(\mathbf{x})\mathbf{d}_{\rm nb}(0) = \frac{0.1}{0.1+\frac{1}{4}\sqrt{x_1^2+x_2^2}}, \quad \mathbf{x}\in[0,4]^2. \quad (38)$$

In order to determine the IC, $\mathbf{d}_{\rm nb}(0)$, Eq. (38) is written for all of the particles in the region $[0,4]^2-\{\mathbf{0}\}$

$$\overline{\boldsymbol{\psi}}_{\rm nb}(\mathbf{x}_J)\mathbf{d}_{\rm nb}(0) = \frac{0.1}{0.1+\frac{1}{4}\sqrt{x_{J1}^2+x_{J2}^2}} - \overline{\psi}_b(\mathbf{x}_J), \quad J = 2,3,...,NP. \quad (39)$$

Eq. (39) provides a system of $NP-1$ linear equations for obtaining the $NP-1$ elements of $\mathbf{d}_{\rm nb}(0)$.

3.2 Temporal discretization

Consider Eq. (36) with the IC obtained from Eq. (39)

$$\mathbf{E}\dot{\mathbf{d}}_{\rm nb} = \mathbf{g}, \quad \mathbf{d}_{\rm nb}(0) \equiv \mathbf{d}_{\rm nb}^0. \quad (40)$$

In the present work, the BDF scheme which is well-known as Gear's implicit multi-step method [Gear (1971)] is utilized to solve this system of nonlinear ODEs. This particular methodology, which is a variable order and variable step scheme, is suitable for solving stiff ODE systems automatically. Even for the cases where the system of ODEs is not stiff, the Gear's method requires less function evaluations than other techniques. Consequently, for the present purposes, it converges faster than most other schemes with comparable or higher degrees of accuracy.

In the BDF scheme, Eq. (40) may be discretized as

$$\mathbf{E}\mathbf{d}_{\rm nb}^n = -\sum_{j=1}^{q}\lambda_{q-j}\mathbf{E}\mathbf{d}_{\rm nb}^{n-j} + \mu_q\Delta t\mathbf{g}^n, \quad (41)$$

where the superscript n over a quantity indicates that the value of the quantity is pertinent to the time step n. In Eq. (41) q is the order of the BDF scheme, λ_{q-j} and μ_q are some coefficients whose values are given by Lambert (1972) and Δt is the time step. For solution of (41), it is necessary to calculate the Jacobian matrix in each time step,

$$\mathbf{J} = -\int_\Omega \overline{\boldsymbol{\psi}}_{\rm nb}^{\rm T}(\overline{\boldsymbol{\psi}}_{\rm nb,1}+\overline{\boldsymbol{\psi}}_{\rm nb,2})f'd\Omega - \int_\Omega \overline{\boldsymbol{\psi}}_{\rm nb}^{\rm T}(u_{,1}+u_{,2})f''\overline{\boldsymbol{\psi}}_{\rm nb}d\Omega - \nu\int_\Omega (\overline{\boldsymbol{\psi}}_{\rm nb,1}^{\rm T}\overline{\boldsymbol{\psi}}_{\rm nb,1}+\overline{\boldsymbol{\psi}}_{\rm nb,2}^{\rm T}\overline{\boldsymbol{\psi}}_{\rm nb,2})d\Omega. \quad (42)$$

The computer program tailored for solving the present problem incorporates the powerful temporal solver by calling the subroutine "DIVPAG" from the IMSL library.

4 Numerical Experiments

In this section, the numerical solution of the BL equation, Eq. (3), subjected to the IC, Eq. (4), and the boundary conditions, Eqs. (5a and b), is investigated. The influence of the diffusion term is examined by considering two very different values of viscosity, ν= 0.5 and 0.025. The dilation parameter associated with the particle J in a given direction is the sum of the distances between particle J and its two adjacent backward and forward particles along that direction. This definition yields variable dilation parameter whenever the particles are distributed non-uniformly.

The convergence behavior is evaluated by computing the L_2 norm

$$\left\|u^R(t)\right\| = \sqrt{\int_0^4 \int_0^4 [u^R(\mathbf{x},t)]^2 dx_1 dx_2}. \qquad (43)$$

4.1 Moderate viscosity: ν = 0.5

Application of the moderate viscosity, ν=0.5, seeks the efficacy of the solution when the diffusion term is important. To this end, 14×14, 20×20, 29×29, 40×40, 56×56, and 79×79 uniformly distributed particles are studied. The convergence behavior of the results at a given time is verified by computing the absolute relative L_2 norm, $\gamma(t)$, defined as

$$\gamma(t) = \left| \frac{\left\|u^R(t)\right\| - \|u^*(t)\|}{\|u^*(t)\|} \right|, \qquad (44)$$

in which $\|u^*(t)\|$ is the L_2norm resulted from the 79×79 particles. The variation of $\gamma(0.6)$, $\gamma(1.2)$, and $\gamma(1.8)$ in terms of the number of particles, NP, have been demonstrated in Fig. 7. It is observed that the convergence rate, which is nearly the same for the depicted cases, increases remarkably with NP.

The profiles of u at t= 0.3, 0.6, 0.9, 1.2, 1.5 and 1.8 employing the 79×79 particles are illustrated in Figs. 8a–c. Interestingly, a high gradient region is captured near the origin. All the profiles are symmetric with respect to the $x_1 = x_2$ plane, as expected. The values of u in the symmetry plane $x_1 = x_2$ at a set of discrete points and different times are presented in Table 1.

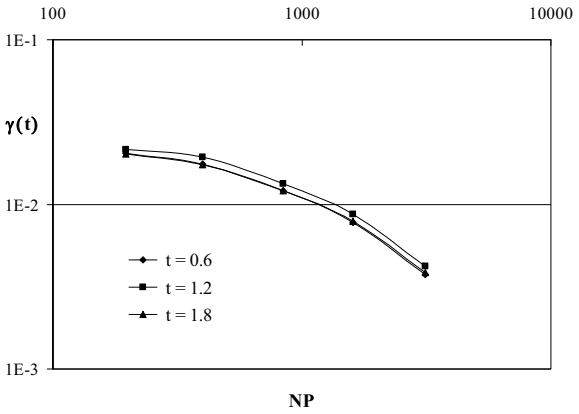

Figure 7: The absolute relative L_2 norm for ν = 0.5

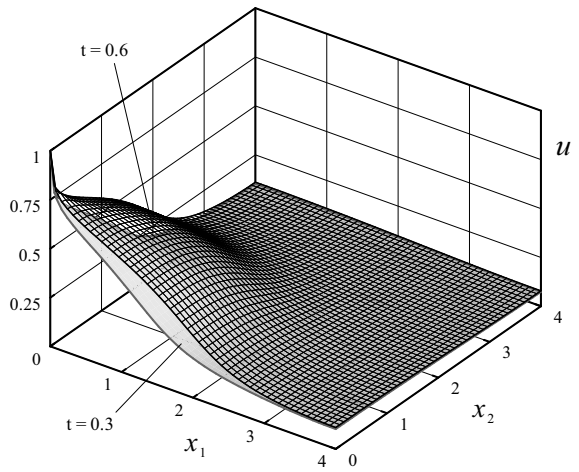

Figure 8a: The profiles of u at t = 0.3 and 0.6 for ν = 0.5, obtained employing 79×79 uniformly spaced particles

4.2 Small viscosity: ν = 0.025

4.2.1 Uniform distribution of particles

In this case, uniformly spaced 14×14, 20×20, 29×29, 40×40, 56×56, and 79×79 particles are considered. For a given distribution of particles,

Table 1: The variation of u in the $x_1 = x_2$ plane for ν= 0.5, obtained employing 79×79 uniformly spaced particles

t / $x_1 = x_2$	0.3	0.6	0.9	1.2	1.5	1.8
0.2	0.675	0.724	0.755	0.777	0.793	0.806
0.4	0.596	0.664	0.704	0.732	0.753	0.769
0.6	0.524	0.614	0.665	0.699	0.724	0.742
0.8	0.446	0.566	0.629	0.669	0.698	0.719
1.0	0.360	0.513	0.593	0.641	0.674	0.698
1.2	0.278	0.451	0.555	0.612	0.650	0.678
1.4	0.217	0.375	0.510	0.582	0.627	0.658
1.6	0.179	0.290	0.455	0.549	0.602	0.638
1.8	0.153	0.218	0.383	0.509	0.575	0.617
2.0	0.136	0.170	0.297	0.457	0.545	0.595
2.2	0.123	0.141	0.218	0.388	0.508	0.571
2.4	0.112	0.123	0.163	0.301	0.459	0.543
2.6	0.103	0.111	0.132	0.217	0.392	0.508
2.8	0.096	0.102	0.114	0.158	0.305	0.462
3.0	0.090	0.095	0.103	0.125	0.217	0.398
3.2	0.084	0.089	0.095	0.108	0.157	0.313
3.4	0.080	0.085	0.090	0.099	0.124	0.227
3.6	0.077	0.082	0.087	0.093	0.108	0.169
3.8	0.075	0.080	0.085	0.091	0.101	0.140
4.0	0.074	0.079	0.084	0.090	0.099	0.131

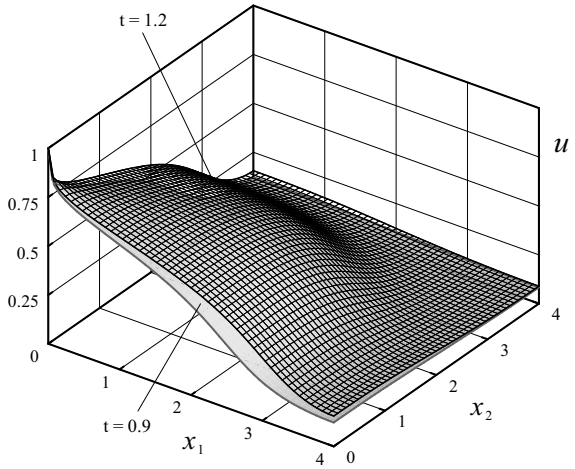

Figure 8b: The profiles of u at $t = 0.9$ and 1.2 for $\nu = 0.5$, obtained employing 79×79 uniformly spaced particles

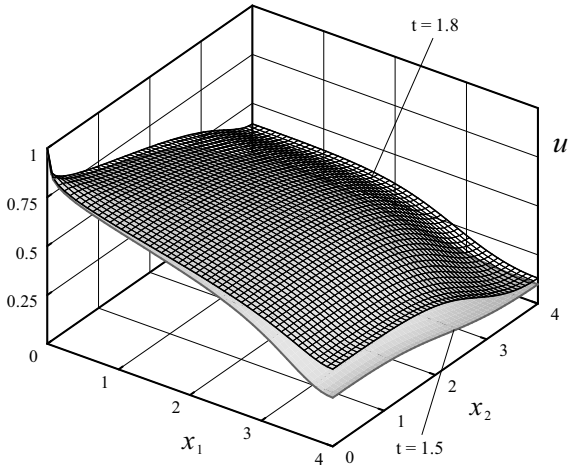

Figure 8c: The profiles of u at $t = 1.5$ and 1.8 for $\nu = 0.5$, obtained employing 79×79 uniformly spaced particles

the L_2 norms for each time t= 1.2 and 1.8 has been computed and plotted versus the number of particles, as illustrated in Figs. 9a and b, respectively.

It is observed that $\left\|u^R(1.2)\right\|$ converges to 1.801 and $\left\|u^R(1.8)\right\|$ approaches 2.433.

For 79×79 particles, the profiles of u at times t=

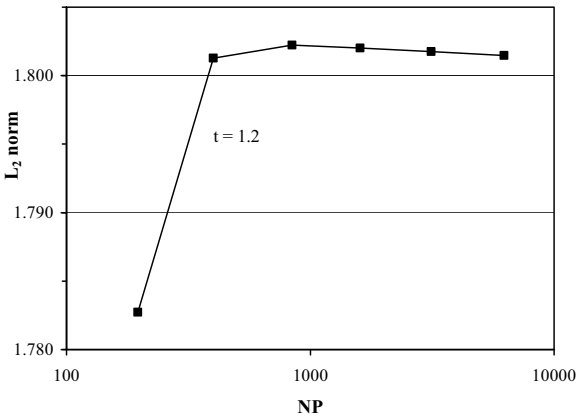

Figure 9a: L_2 norm at $t = 1.2$ for $\nu = 0.025$

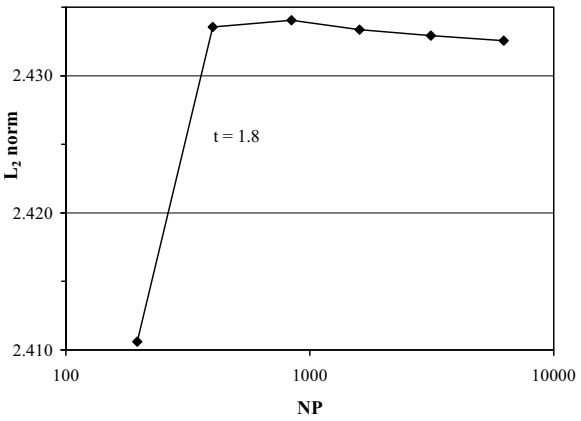

Figure 9b: L_2 norm at $t = 1.8$ for $\nu = 0.025$

0.6, 1.2 and t=1.8, 2.1 are displayed in Figs. 10a and b, respectively. It is observed that the sharp gradient which forms at the early stages becomes steeper with time as it travels towards the corner (4, 4). In order to demonstrate that the results are free of any artifacts, the most critical regions in the neighborhoods of the jumps at times t= 1.8, 2.1 are magnified, Figs. 11–12. For t= 2.1, very few insignificant overshootings and undershootings in the vicinities of the sharp gradient region are detected, whereas for t= 1.8 no such a phenomenon occurs. It is should be noted that the maximum gradient occurs in the $x_1 = x_2$ plane; the corresponding values of u for ν = 0.025, t= 0.6, 1.2, 1.8, and 2.1 are compared using 79×79 uniformly distributed particles and are displayed in Table 2.

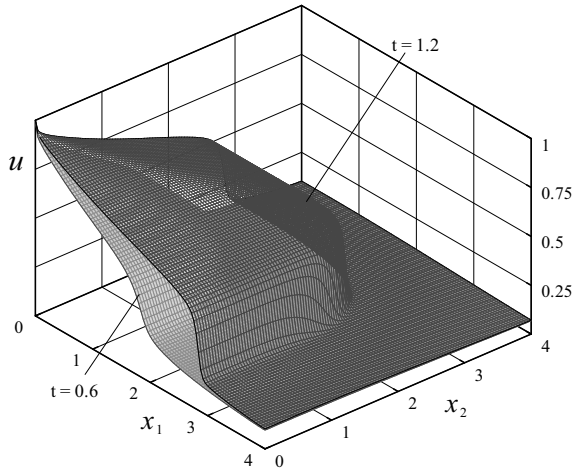

Figure 10a: The profiles of u at $t = 0.6$ and 1.2 for $\nu = 0.025$, obtained employing 79×79 uniformly spaced particles

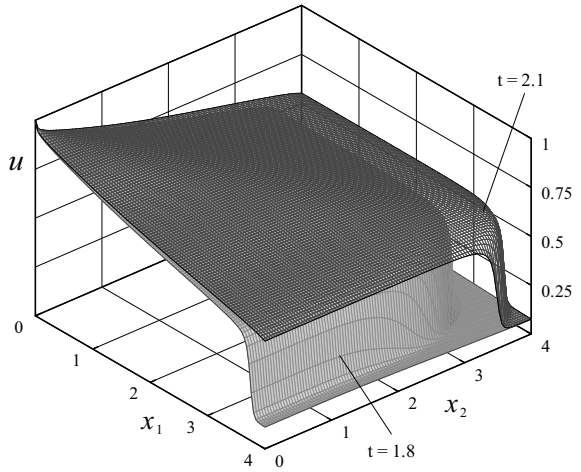

Figure 10b: The profiles of u at $t = 1.8$ and 2.1 for $\nu = 0.025$, obtained employing 79×79 uniformly spaced particles

4.2.2 Non-uniform distribution of particles

Consider the region $[0, 4]^2$. 3136 particles are non-uniformly distributed throughout this region in a fashion shown in Fig. 13. In this distribution the maximum and minimum interparticle spacing are 2.48 $\Delta\overline{x}$ and 0.78 $\Delta\overline{x}$ in the regions $[0, 1.4]^2$ and $[3.2, 3.6]^2$, respectively; where $\Delta\overline{x}$= 0.0513 is pertinent to the distance between the adjacent particles when 79×79 (6241) uniformly spaced particles are utilized over $[0, 4]^2$.

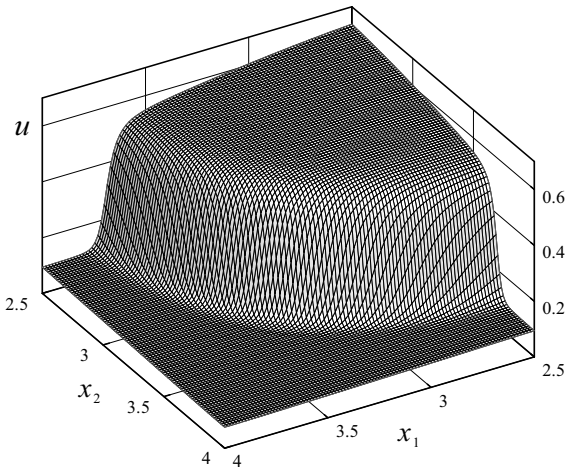

Figure 11: The magnified profile of u near the front at $t = 1.8$ for $\nu = 0.025$, obtained employing 79×79 uniformly spaced particles

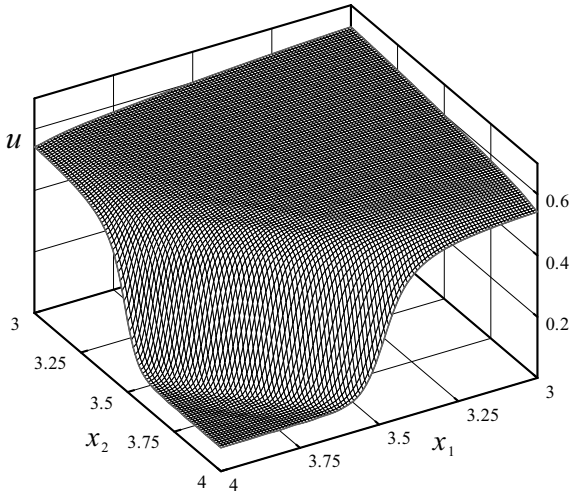

Figure 12: The magnified profile of u near the front at $t = 2.1$ for $\nu = 0.025$, obtained employing 79×79 uniformly spaced particles

Employing this non-uniform distribution, the L_2 norms corresponding to times t= 0.6, 1.2, 1.8, and 2.1 have been computed by GRKPM and presented in Table 3. For comparison, the L_2 norms using 79×79 (6241) uniformly spaced particles are also given. It is observed that for $t \leq 1.8$, the L_2 norms associated with the 3136 non-uniformly distributed particles are very close to those of 6241 uniformly spaced particles; the absolute relative L_2 norm, γ, decreases as time increases. In

Table 2: The variation of u in the $x_1 = x_2$ plane for ν= 0.025, obtained employing 79×79 uniformly spaced particles

t / $x_1 = x_2$	0.6	1.2	1.8	2.1
0.2	0.841	0.881	0.902	0.909
0.4	0.777	0.838	0.868	0.878
0.6	0.722	0.801	0.839	0.851
0.8	0.671	0.768	0.812	0.827
1.0	0.622	0.737	0.788	0.805
1.2	0.571	0.708	0.765	0.784
1.4	0.507	0.680	0.744	0.765
1.6	0.286	0.653	0.723	0.746
1.8	0.173	0.626	0.703	0.728
2.0	0.147	0.598	0.684	0.711
2.2	0.130	0.568	0.666	0.694
2.4	0.117	0.527	0.647	0.678
2.6	0.107	0.122	0.628	0.661
2.8	0.099	0.109	0.609	0.645
3.0	0.092	0.099	0.589	0.629
3.2	0.086	0.091	0.567	0.613
3.4	0.080	0.085	0.105	0.596
3.6	0.076	0.080	0.084	0.577
3.8	0.072	0.075	0.079	0.156
4.0	0.070	0.073	0.076	0.078

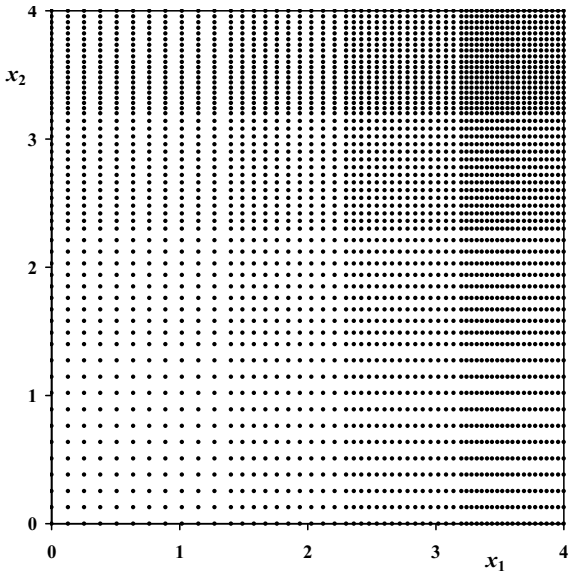

Figure 13: The positions of the 3136 non-uniformly distributed particles for $\nu = 0.025$

Table 3: Comparison of the L_2 norms for ν= 0.025

t	6241 uniformly spaced particles	3136 non-uniformly distributed particles	
	L_2 norms	L_2 norms	γ (%)
0.6	1.17023	1.17011	0.010
1.2	1.80148	1.80138	0.006
1.8	2.43257	2.43257	0.000
2.1	2.69763	2.69832	0.026

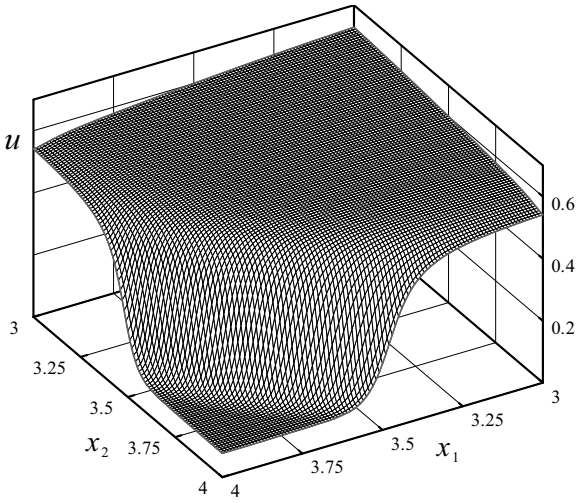

Figure 14: The magnified profile of u near the front at $t = 2.1$ for $\nu = 0.025$, obtained employing the 3136 non-uniformly distributed particles; see Fig. 13

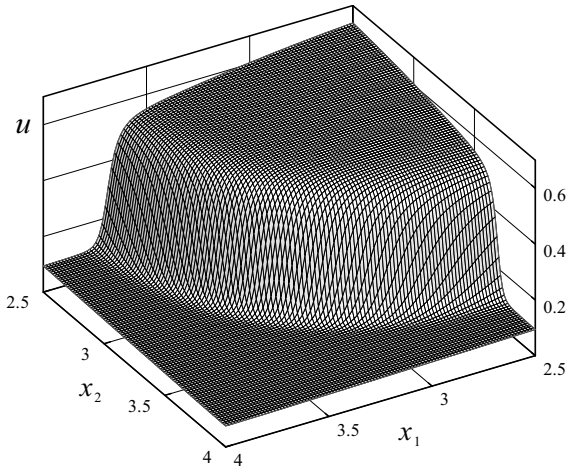

Figure 15: The magnified profile of u near the front at $t = 1.8$ for $\nu = 0.025$, obtained employing the 3136 non-uniformly distributed particles; see Fig. 13

the worst case (t= 0.6), γ is only 0.010%. The best agreement between the results happens at t= 1.8 where γ= 0.000%. At t=2.1, γ takes on a larger value (0.026%). This may be due to the inaccuracy of the solution, specially near the front, when the particles are distributed uniformly. A magnified snap shot of u at time t=2.1 obtained employing the 3136 non-uniformly distributed particles is displayed in Fig. 14. As it is observed, no noticeable spurious overshooting and undershooting occur. While Fig. 12, pertinent to 6241 uniformly spaced particles and t=2.1, displays few overshootings and undershootings. This is due to the fact that the number of particles in the critical region $[3,4]^2$ for the non-uniform case is 30% more than the number of particles for the uniform case. On the other hand, for the case of uniform distribution of particles, an excessive number of particles are allocated to the regions far from the critical zone, rendering them essentially useless. Fig. 15 which demonstrates the profile of $u(\mathbf{x}, 1.8)$ for $\mathbf{x} \in [2.5,4]^2$ obtained employing the non-uniform distribution is distinguishably smooth, even near the steep front.

Table 4 presents the values of u in the $x_1 = x_2$ plane at times t=1.8 and 2.1. At t=1.8 and $x_1 = x_2$=3.2, there is a slight discrepancy (0.001) between the results pertinent to the 3136 and 6241 non-uniformly and uniformly distributed particles, respectively. At t=2.1 the discrepancy of 0.001 occurs at $x_1 = x_2$=3.4 and 3.6, moreover, the maximum difference of 0.008 is observed for $x_1 = x_2$=3.8.

The expended CPU time corresponding to 6241 uniformly spaced particles is 3.2 times the CPU time consumed for the 3136 non-uniformly distributed particles. This feature in addition to more accurate and smooth results produced using the 3136 particles demonstrate that the non-uniform distribution of particles, with about half the number of particles utilized for the case of uniformly spaced particles, is much more efficient.

Table 4: Comparison of the u values in the $x_1 = x_2$ plane for ν= 0.025

t	1.8		2.1	
$x_1 = x_2$	3136 non-uniformly distributed particles	6241 uniformly spaced particles	3136 non-uniformly distributed particles	6241 uniformly spaced particles
2.4	0.647	0.647	0.678	0.678
2.6	0.628	0.628	0.661	0.661
2.8	0.609	0.609	0.645	0.645
3.0	0.589	0.589	0.629	0.629
3.2	0.566	0.567	0.613	0.613
3.4	0.105	0.105	0.595	0.596
3.6	0.084	0.084	0.576	0.577
3.8	0.079	0.079	0.148	0.156
4.0	0.076	0.076	0.078	0.078

5 Conclusions

The function reconstruction of a typical third order polynomial in a two-dimensional region demonstrates that GRKPM which is somewhat indifferent to the dilation parameter gives much more accurate result with considerably lower CPU time than RKPM. Moreover, the convergence rate in GRKPM is double its counterpart in RKPM.

The 2D GRKPM in conjunction with the Gear's method which is applied for solution of the viscous BL equation works well for both the moderate and small values of viscosity. Therefore, the methodology is efficient not only when the diffusion term is important, but also when the diffusion term is small and steep gradient regions develop. For uniformly distributed particles, the proposed method converges rapidly by increasing number of particles. Nevertheless, the non-uniform distribution of particles with high concentration in critical regions and dispersed distribution away from such regions not only leads to more accurate and smooth results but also consumes remarkably lower CPU time.

The high performance of the proposed method in solving the 2D BL equation reveals its high potential for treating nonlinear evolutionary partial differential equations exhibiting high gradients.

Acknowledgement: This work was in part supported by the center of excellence in structures and earthquake engineering at Sharif University of Technology.

References

Atluri, S.N.; Cho, J.Y.; Kim, H.G. (1999): Analysis of thin beams, using the meshless local Petrov-Galerkin method, with generalized moving least squares interpolations. *Comput Mech*, vol. 24, pp. 334-347.

Atluri, S.N.; Han, Z.D.; Rajendran, A.M. (2004): A new implementation of the meshless finite volume method, through the MLPG "mixed" approach. *CMES: Computer Modeling in Engineering & Sciences*, vol. 6, pp. 491-513.

Atluri, S.N.; Liu, H.T.; Han, Z.D. (2006a): Meshless local Petrov-Galerkin (MLPG) mixed collocation method for elasticity problems. *CMES: Computer Modeling in Engineering & Sciences*, vol. 14, pp. 141-152.

Atluri, S.N.; Liu, H.T.; Han, Z.D. (2006b): Meshless local Petrov-Galerkin (MLPG) mixed finite difference method for solid mechanics. *CMES: Computer Modeling in Engineering & Sciences*, vol. 15, pp. 1-16.

Atluri, S.N.; Shen, S. (2002a): The Meshless Local Petrov-Galerkin (MLPG) Method, Tech Science Press, New York.

Atluri, S.N.; Shen, S. (2002b): The meshless local Petrov-Galerkin (MLPG) method: A simple & less costly alternative to the finite element and boundary element method. CMES: *Computer Modeling in Engineering & Sciences*, vol. 3, pp.

11-52.

Atluri, S.N.; Shen, S. (2005): Simulation of a 4th order ODE: illustration of various primal & mixed MLPG methods. *CMES: Computer Modeling in Engineering & Sciences*, vol. 7, pp. 241-268.

Atluri, S.N.; Zhu, T. (1998): A new meshless local Petrov-Galerkin (MLPG) approach in computational mechanics. *Comput Mech*, vol. 22, pp. 117-127.

Aziz, k.; Settari, A. (1979): Petroleum Reservoir Simulation, Applied Science Publishers, London.

Babuška, I.; Melenk, J. (1997): The partition of unity method. *Int J Numer Methods Eng*, vol. 40, pp. 727-758.

Belytschko, T.; Lu, Y. Y.; Gu, L. (1994a): Element-free Galerkin methods. *Int J Numer Methods Eng*, vol. 37, pp. 229-256.

Belytschko, T.; Lu, Y. Y.; Gu, L. (1994b): Fracture and crack growth by element-free Galerkin method. *Model Simul Mater Sci Eng*, vol. 2, pp. 519-534.

Berger, M.; Oliger, J. (1984): Adaptive mesh refinement for hyperbolic partial differential equations. *J Comput Physics*, vol. 53, pp. 484-512.

Buckley, J. M.; Leverett, M. C. (1942): Mechanism of fluid displacement in sands. *Trans AIME*, vol. 146, pp. 107-116.

Chen, J. S.; Pan, C.; Wu, C. T.; Liu, W. K. (1996): Reproducing kernel particle methods for large deformation analysis of non-linear structures. *Comput Methods Appl Mech Eng*, vol. 139, pp. 195-227.

Cho, J. Y.; Atluri, S. N. (2001): Analysis of shear flexible beams, using the meshless local Petrov-Galerkin method, based on a locking-free formulation. *Eng Comput*, vol. 18, pp. 215-240.

Durate, C. A.; Oden, J. T. (1996): An h-p adaptive method using clouds. *Comput Methods Appl Mech Eng*, vol. 139, pp. 237-262.

Gear, C. W. (1971): Numerical Initial Value Problems in Ordinary Differential Equations, Prentice-Hall, Englewood Cliffs.

Gelinas, R. J.; Doss, S. K.; Miller, K. (1981): The moving finite element method: applications to general partial differential equations with multiple large gradients. *J Comput Physics*, Vol. 40, pp. 202-249.

Hashemian, A. (2000): A Study of Columns' Buckling Loads and Modes by Meshfree Methods, Master's Thesis, Sharif University of Technology, Tehran.

Hashemian, A.; Shodja, H. M. (2008a): Gradient reproducing kernel particle method. *J Mech Mater Sturct*, vol. 3, pp. 127-152.

Hashemian, A.; Shodja, H. M. (2008b): A meshless approach for solution of Burgers' equation. *J Comput Appl Math*, vol. 220, pp. 226-239.

Johnson, I. W.; Wathen, A. J.; Baines, M. J. (1988): Moving finite element methods for evolutionary problems, II, applications. *J Comput Physics*, vol. 79, pp. 270-297.

Lambert, J. D. (1972): Computational Methods in Ordinary Differential Equations, John Wiley & Sons, New York.

Li, S.; Liu, W. K. (2002): Meshfree and particle methods and their applications. *Appl Mech Rev*, vol. 55, pp. 1-34.

Li, H.; NG, T. Y.; Cheng, J. Q.; Lam, K. Y. (2003): Hermite–Cloud: a novel true meshless method. *Comput Mech*, vol. 33, pp. 30-41.

Liu, W. K.; Jun, S.; Zhang, Y. F. (1995): Reproducing kernel particle methods. *Int J Numer Methods Fluids*, vol. 20, pp. 1081-1106.

Liu, W. K.; Chen, Y. J.; Uras, R. A.; Chang C. T. (1996): Generalized multiple scale reproducing kernel particle methods. *Comput Methods Appl Mech Eng*, vol. 139, pp. 91-158.

Long, S.; Atluri, S. N. (2002): A meshless local Petrov-Galerkin method for solving the bending problem of a thin plate. *CMES: Computer Modeling in Engineering & Sciences*, vol. 3, pp. 53-63.

Lucy, L. B. (1977): A numerical approach to the testing of the fission hypothesis. *Astron J*, vol. 82, pp. 1013-1024.

Nayroles, B.; Touzot, G.; Villon, P. (1992): Generalizing the finite element method: diffuse approximation and diffuse elements. *Comput Mech*, vol. 10, pp. 307-318.

Parker, J. C. (1989): Multiphase flow and transport in porous media. *Rev Geophysics*, vol. 27,

pp. 311-328.

Raju, I. S.; Phillips , D. R. (2003): Further developments in the MLPG method for beam problems. *CMES: Computer Modeling in Engineering & Sciences*, vol. 4, pp. 141-159.

Rivière, B.; Bastian, P. (2004): Discontinuous Galerkin Methods for Two-Phase Flow in Porous Media, Technical Report 2004-28, University of Heidelberg.

Shodja, H. M.; Hashemian, A. (2007a): A remedy to gradient type constraint dilemma encountered in RKPM. *Adv Eng Softw*, vol. 38, pp. 229-243.

Shodja, H. M.; Hashemian, A. (2007b): 2-D GRKPM: analysis of the Kirchhoff plate. In: A. Ferreira, G. Fasshauer, E. Kansa, V. M. A. Leitão (eds) *Second ECCOMAS thematic conference on meshless methods*. Faculty of Engineering of the University of Porto, Porto, pp. 286-293.

Wagner, G. J.; Liu, W. K. (2000): Application of essential boundary conditions in mesh-free methods: a corrected collocation method. *Int J Numer Methods Eng*, vol. 47, pp. 1367-1379.

Zhu, T.; Atluri, S. N. (1998): A modified collocation method and a penalty formulation for enforcing the essential boundary conditions in the element free Galerkin method. *Comput Mech*, vol. 21, pp. 211-222.

Zhu, T.; Zhang, J. D.; Atluri, S. N. (1998a): A local boundary integral equation (LBIE) method in computational mechanics, and a meshless discretization approach. *Comput Mech*, vol. 21, pp. 223-235.

Zhu, T.; Zhang, J. D.; Atluri, S. N. (1998b): A meshless local boundary integral equation (LBIE) method for solving nonlinear problems. *Comput Mech*, vol. 22, pp. 174-186.